ELSEVIER

Cement & Concrete Composites 23 (2001) 289–297

Cement & Concrete Composites

www.elsevier.com/locate/cemconcomp

Towards a model of concrete mesostructure

Anne-Sophie Dequiedt [a], Michel Coster [a], Jean-Louis Chermant [a,*], Dominique Jeulin [b]

[a] LERMAT, URA CNRS 1317, ISMRA, 6 bd Maréchal Juin, 14050 Caen Cedex, France
[b] Centre de Morphologie Mathématique, EMP, 35 rue St Honoré, 77305 Fontainebleau, France

Abstract

This short paper will present a two-dimensional (2D) model of concrete material, based on probabilistic models: it is a combination of a Voronoi tessellation for the gravel, followed by a Boolean model of spherical grains for the air-voids, with elimination of the air-voids–gravel intersections so that there is no contact between them. The model was tested via crossed-covariance. Results on true and simulated structures are in good agreement. This is a first step towards a 3D model.

Keywords: Simulation; Voronoi tessellation; Boolean model; Crossed-covariance

1. Introduction

At the mesoscopic scale, a normal concrete is made of three phases: polyhedral gravel, and spherical pores (air-voids) in a mortar matrix (Fig. 1). Some morphological characteristics of these constituents are accessible by image analysis on plane sections of that material. Stereology provides access to some parameters in $\mathbb{R}^3$ such as the phase ratio, the specific surface area and the mean free path, from measurements in $\mathbb{R}^2$. On the contrary, it is illusory to attempt topological parameters or distances between particles [1–3]. To estimate such parameters, modelling of the material is essential.

In the case of concrete, the constraints are large enough: multiphased aspect of the material, existence of several scales of pertinence, etc. Analysis with covariance functions [3,4] are of a great help: they can facilitate the choice of a possible probabilistic model [5].

The interest to model a structure of concrete will be to obtain the distances between air-voids (V) in $\mathbb{R}^3$ space, as these distances are directly related to the freeze–thaw resistance of these materials [6,7].

In this paper, concrete morphologically investigated in our laboratory [8–11] will be modelled using automatic image analysis methods. In a first step, we will limit this work to $\mathbb{R}^2$ space and only three phases will be considered: air-voids, gravel and matrix (i.e., cement paste + sand).

Gravel will be simulated from a Voronoi tessellation which must be eroded, then opened. The air-void set will be represented by a Boolean model of spherical primary grains. In order to validate this simulation, probabilistic characteristics obtained from the Choquet's capacity [12] will be measured [13].

2. Materials

Blocks of microconcrete ($4 \times 4 \times 16$ cm^3 in size) were fabricated by the classical procedure, with (0.03 wt%) and without air entraining agent (AEA): cement 450 g/l, gravel 800 g/l, sand 1200 g/l, water/cement 0.5 wt%. Observations and morphological analysis were performed on thick slices (5×5 cm^2) cut in each block after one month of curing. These slices were embedded under vacuum by a green fluorescent resin and then ground.

Automatic image analysis was performed with Aphelion software (ADCIS, Caen, France).

3. Construction of the model

Due to the very different structure of gravel (G) and air-voids (V), the proposed models will involve two steps. In the first one, gravel will be simulated, then the simulation of air-voids will be undertaken. All the basic notions of image analysis utilized in this paper are in the first paper of this special issue [14].

* Corresponding author.

0958-9465/01/$ - see front matter
PII: S0958-9465(00)00057-3

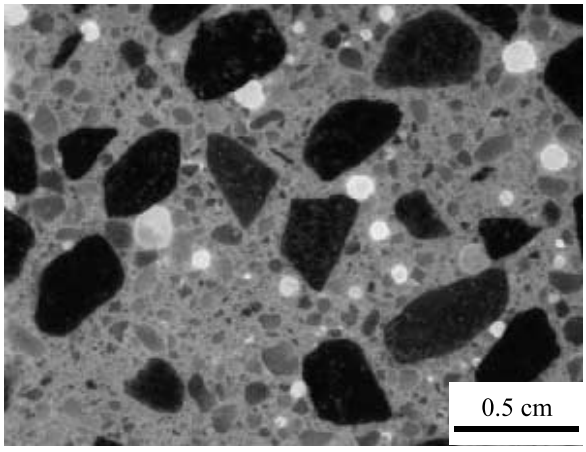

Fig. 1. Optical micrograph of a concrete. In dark: gravel; in grey: matrix (cement paste + sand); in white: air-voids.

3.1. Simulation of gravel and analysis of Choquet's capacity

The set of gravel is made of a set of grains more or less rounded, clearly separated from each other by the mortar (cement paste + sand). To obtain such a random structure, one can start from a space tessellation: here, one has chosen to utilize the tessellation of Voronoi.

It can be described as the complementary of the skeleton by influence zone (SKIZ) of a point Poisson process. This tessellation encompasses all the space (Fig. 2). So, to obtain disconnected grains, they must be eroded. In such conditions, convex but polyhedral grains are obtained. To form rounded grains, an opening on the previous result must be performed.

A visual observation of the first test in $\mathbb{R}^2$ has shown that this simulation gave a plausible image in choosing an erosion and opening step which leads to the disappearance of the smallest classes of the tessellation. Thus, the distance between gravel is not constant, which is closer to reality.

Three parameters are required for a such simulation. They are:

- the density θ of the Poisson process,
- the erosion step, λ_1, related to the minimum distance between gravel,
- the opening step, λ_2, related to the minimum curvature of the gravel.

In any simulation, the edge effect of the frame of measurements can pose some problems. To avoid any bias, only the central part of the image will be used.

So, the algorithm of simulation will be as follows:

- to set N seeds, N being given by a point Poisson process of density θ, higher than the desired density; it will correspond to I_1,
- complementation of the SKIZ: $I_1 \rightarrow I_2$,
- erosion of size $\lambda_1 \rightarrow I_3$,
- opening of size λ_2 by the disk: $\rightarrow I_4$,
- erosion of the full mask by the image of size $2(\lambda_1 + 2\lambda_2) - 2 :\rightarrow I_5$,
- intersection of I_4 and I_5: $\rightarrow I_{\text{final}}$.

The three parameters to be determined are: the number of seeds, N, to implement (or the density, θ), and the steps of erosion, λ_1, and of opening, λ_2. They are chosen in order to obtain the ratio and the number of grains experimentally obtained. In our case, they were $V_V(G) = 30\%$ for the volume fraction of gravel and a mean of 23.25 grains per image (40×40 mm^2).

To determine these three parameters – θ, λ_1 and λ_2 – two were held constant and the third varied. Then, the best adapted parameters to represent this series are: $\theta = 95$; $\lambda_1 = 8$ and $\lambda_2 = 14$. Fig. 3 shows an image of simulated gravel.

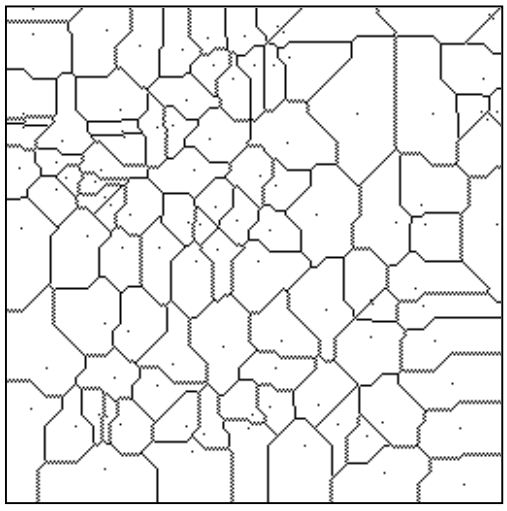

Fig. 2. Example of a Voronoi tessellation in $\mathbb{R}^2$.

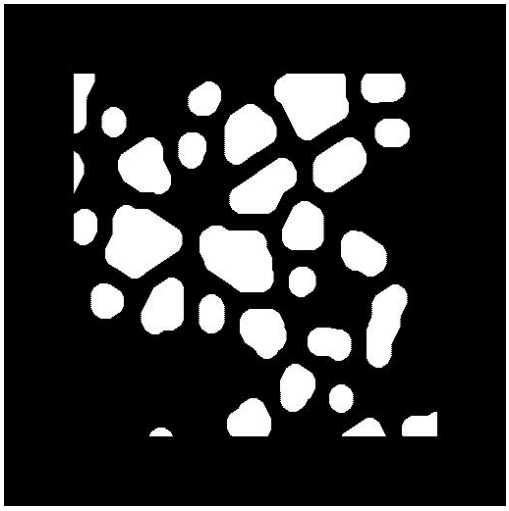

Fig. 3. Simulated image of gravel with $V_V(G) = 0.3$.

For such a model, the theoretical relationships of the Choquet's capacity [4,5,13], corresponding to the probability for a set K to intersect the investigated random set A, are not known. Hence, one must undertake a simulation to estimate the theoretical Choquet's capacity, and to compare the results to the measurements on this material.

The simple covariance (or probability for two parts x and $x+h$ to be in the same phase [3–5], $C(h)$) of the simulated gravel is measured in order to compare with the results on "real" images (Fig. 4). First, one notes that before reaching the asymptote, the covariance on the simulated structures passes through a local minimum for $h=p$, which is also effectively observed on the covariances estimated for that material. Nevertheless, $C(p)$ lays higher than the asymptote value for the simulation.

Values of the specific surface area, $S_V(G)$, were determined from the slopes at the origin of the covariances. One obtains 0.42 mm^{-1} on real images, and 0.40 mm^{-1} on simulated images: this is an acceptable result.

So, this model seems to be a plausible approach to represent gravel in our specimens.

3.2. Simulation of air-voids

To simulate air-voids, the two series of concrete materials were considered: with and without air entraining agent (AEA).

The structure of air-voids is represented by a Boolean model with spherical grains. The Boolean model is defined from a set of primary grains A' from which the geometry and the size distribution are known. These primary grains reconstituted by their centres are implemented (set in the space) according to a point Poisson process. The union represents the Boolean models.

In the case of a Boolean model, the analytical laws related to the Choquet's capacity $Q(K)$ are known [4,5,13,15], specially for compacts K of simple geometry such as the disk, the hexagon $H(r)$ of side r, the segment of straight line ℓ, or the bi-point h. Then, one can theoretically verify the model in analyzing the Choquet's capacity of the complementary set of the air-voids.

Now, one must verify the linearity of $\ln(Q(\ell))$ and of $1/r\ln(Q(H(r))/q)$, where q represents the ratio of the complementary phase of the set to be analyzed [5]. Using the bi-point, h allows one to calculate the mean geometrical covariogram [4,16]:

$$K(h) = V(A' \cap A'_h). \tag{1}$$

In the case of a Boolean model, the reduced mean geometrical covariogram:

$$r(h) = \overline{K}(h)/\overline{K}(0) \tag{2}$$

must be monotonous, decreasing and always positive.

Nevertheless, in our particular case, the air-voids appear only in the complementary set of the gravel. The Boolean model will then be intersected by the complementary set of the gravel. In that case, one does not need to determine the Choquet's capacity of the complementary set of the air-voids, but that of the complementary set of the observed air-voids, i.e., of the matrix in the complementary set of gravel. Of course, one supposes that the observed air-voids, $V_V(V)_{obs}$, are the intersection of a Boolean model A with the complementary set of the gravel, G^C:

$$V_{obs} = A \cap G^C. \tag{3}$$

As tests are generally carried out on the complementary of the analyzed set, it is equivalent to:

$$M = A^C \cap G^C, \tag{4}$$

where M is the matrix.

Supposing the independence between A^C and G^C, one thus has:

$$P\{K \subset M\} = P\{K \subset A^C\}P\{K \subset G^C\}, \tag{5}$$

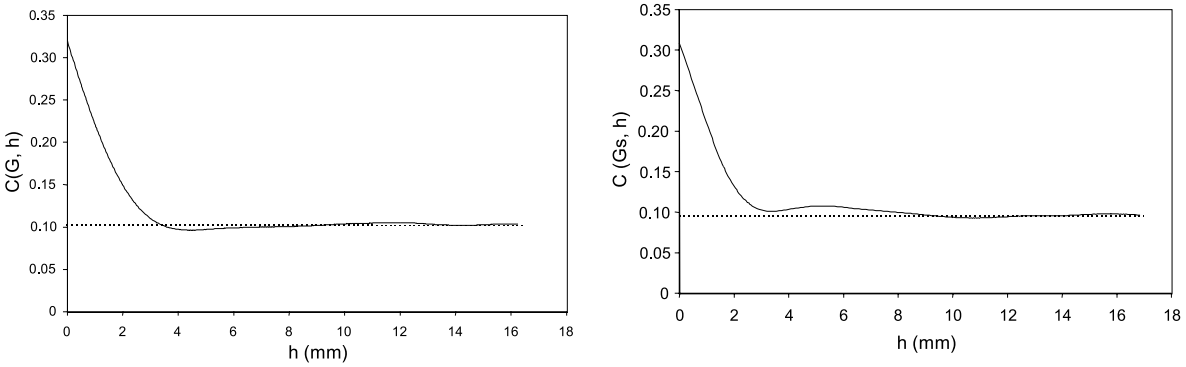

(a) Covariance on "real" images ". **(b)** Covariance on simulated images.

Fig. 4. Comparison of the covariances of gravel on real (a) and simulated (b) images.

then:

$$P\{K \subset A^{C}\} = \frac{P\{K \subset M\}}{P\{K \subset G^{C}\}}, \tag{6}$$

where A^{C} represents the complementary of the Boolean model if $Q(K) = A_A(E^K(M))/A_A(E^K(G^{C}))$ verifies the analytical laws of a Boolean model. It is equivalent to investigate the eroded set of the matrix, $E^K(M)$, in a particular frame of measurements: the complementary set of gravel, G^{C}. In that case, one can calculate $Q(K)$ as:

$$\overline{Q}(K) = \frac{\sum_i A(G_i^{C}) Q(K)_i}{\sum_i A(G_i^{C})}, \tag{7}$$

where i is the number of the image, and $Q(K)_i = A_A(E^K(M))_i$.

$Q(\ell)$ and $Q(H(r))$ are then calculated according to Eq. (7), and the reduced mean geometrical covariogram $r(h)$ from the covariance. Fig. 5 shows the function $\ln(Q(\ell))$ and $1/r\ln(Q(H(r))/Q)$ of the two investigated series. Some covariograms are presented in Fig. 6.

The correspondence of the analytical relationships of a Boolean model and the experimental Choquet's capacity is not perfect. The linearity for ℓ disappears for values higher than 14 mm in the case of the series with AEA. The linearity for $H(r)$ is strictly verified only for the series without AEA. Moreover, the mean geometrical covariogram which should remain positive, slightly passes below the asymptote quickly enough for the series with AEA, while for the series without AEA there is a change further.

In spite of these restrictions, we have sought to construct a model of air-voids from a Boolean model.

Two characteristics must be determined: the law of distribution of primary grains and the Poisson density, θ'. As air-voids are appearing only in the complementary set of the gravel, the Boolean model will be intersected in that complementary set.

As this outline of the model is limited to $\mathbb{R}^2$ space, the law of distribution of air-voids will be represented from the experimental granulometry analysis of the air-voids. An exponential law of type:

$$f(\lambda) = \frac{1}{b}\exp(-\lambda/b), \tag{8}$$

where λ corresponds to the diameter of spherical air-voids, represents fairly well this distribution (Fig. 7).

The density of implemented points must be higher than the experimental density, as this one takes only into account the air-voids inside the matrix (real air-voids). It turns out that the number of points to be implemented in the total image is, respectively, 120 for the series without AEA, and 300 with AEA.

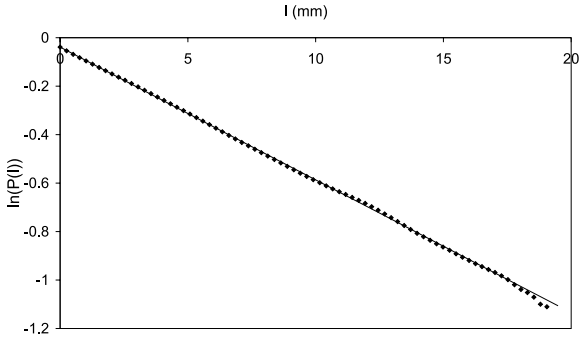

(a) ln(Q(ℓ)) of the series without AEA

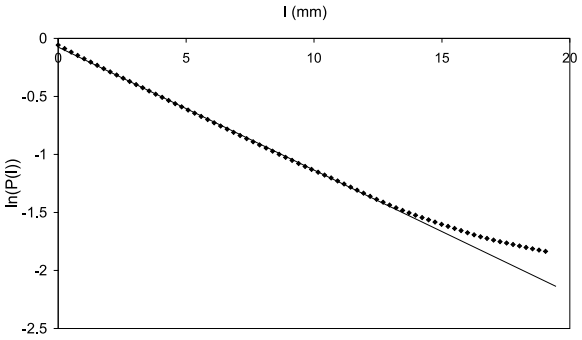

(b) ln(Q(ℓ)) of the AEA series

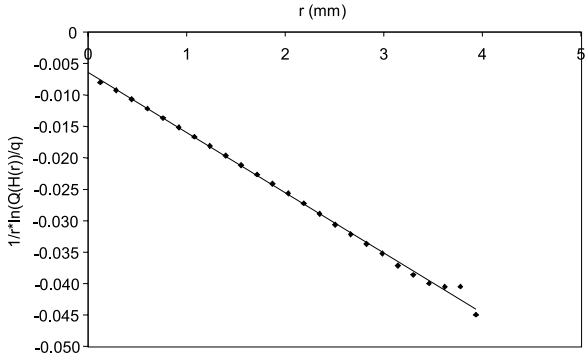

(c) 1/r*ln(Q(H(r))/q) of the series without AEA

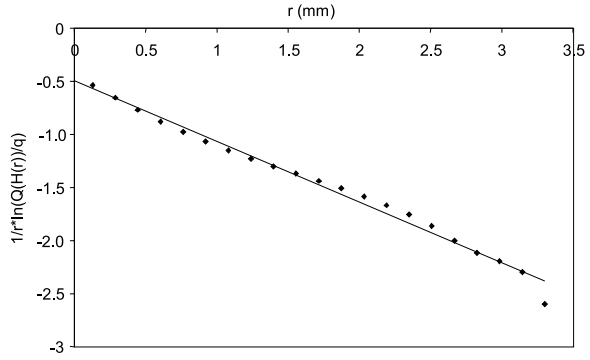

(d) 1/r*ln(Q(H(r))/q) of the series with AEA

Fig. 5. Verification of the linearity of the analytical laws $\ln(Q(\ell))$ and $1/r\ln(Q(H(r))/Q)$.

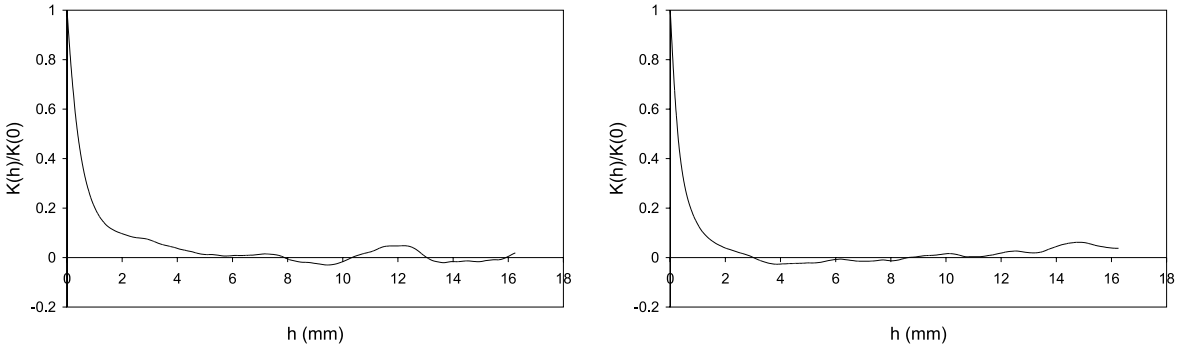

(a) Series without AEA **(b)** Series with AEA

Fig. 6. Experimental mean geometrical covariogram of the two series of concrete investigated, with and without air entraining additive (AEA).

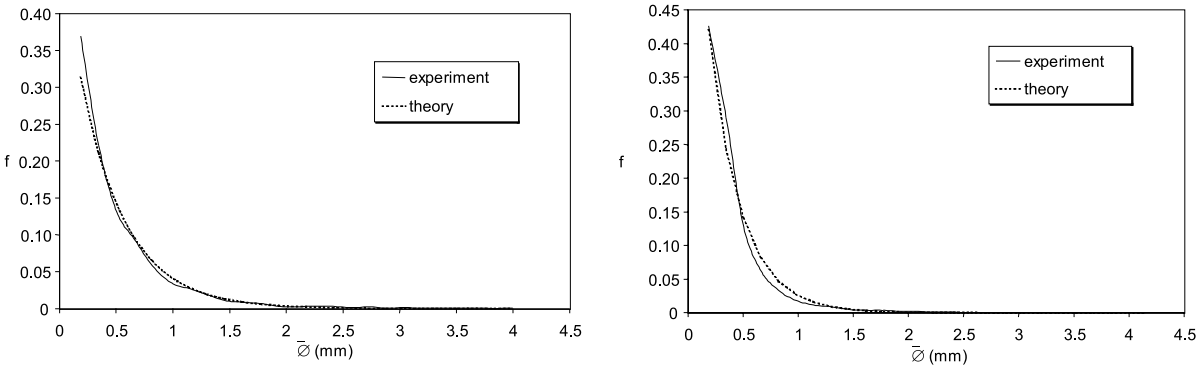

(a) Series without AEA
Theoretical law: $f(\lambda) = 0.5 \exp(-\lambda/0.4)$

(b) Series with AEA
Theoretical law: $f(\lambda) = 0.8 \exp(-\lambda/0.29)$

Fig. 7. Modelling of the distributions of diameters of air-voids of the two different series of concrete by an exponential law.

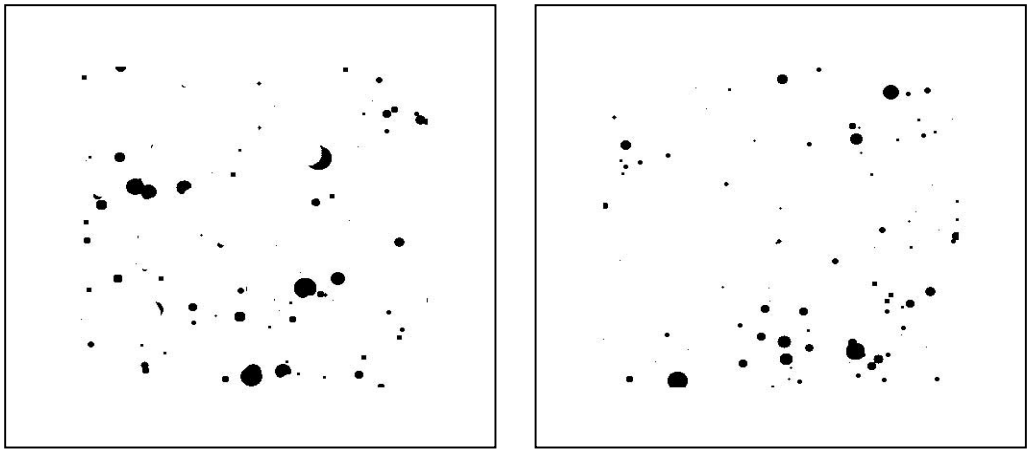

(a) **(b)**

Fig. 8. Image of simulated air-voids: (a) the intersections of air-voids and gravel are eliminated (I'_2); (b) the air-voids simulation (I'_3).

At that step of the construction of the model, one notices that some air-voids are partially hidden by gravels, which is not in agreement with the reality. So the simulation has been slightly modified in eliminating air-voids intersected by gravel, as has been shown by Dequiedt [8,11]. So the following algorithm has been developed (Fig. 8):

- to set, in the total image, a Boolean model of spherical air-voids of density θ' with a law of distribution of exponential diameters of parameters a and b: $\rightarrow I'_1$,

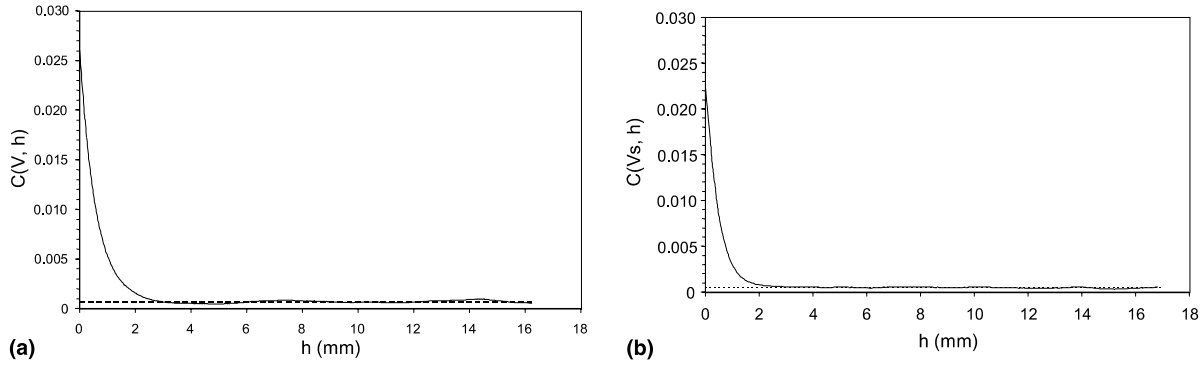

Fig. 9. Comparison of the covariances of air-voids on real and simulated images.

- to reconstruct I'_1 from the image of the simulated gravel: $\rightarrow I'_2$,
- to make the difference between I'_1 and $I'_2 \rightarrow I'_3$.

In order to validate this model, the simple covariances of these simulated air-voids were measured and compared with those on real images (Fig. 9). The values of the ratios and specific surface areas are given in Table 1. From these results, it appears that this model seems to be convenient.

Figure 10 presents a visual comparison between a real image with the three phases (air-void, gravel and matrix), and a simulated image for the series of materials without AEA.

Table 1
Comparison of air-voids ratio, $V_V(V)$ and of the specific surface area, $S_V(V)$, of real and simulated air-voids

	Real images		Simulated images	
	Without AEA	With AEA	Without AEA	With AEA
$V_V(V)$	0.03	0.04	0.02	0.04
$S_V(V)$ (mm^{-1})	0.15	0.31	0.13	0.28

4. Discussion: analysis of the model by covariances

To confirm the validation of the model, the behavior of each phase with regard to the others was approached from the crossed-covariances [3,4,14,16] between the different phases. In a first step, the covariances $C(X_i : X_j, k)$ and $C(X_j : X_i, k)$ were calculated separately: one notes that they are similar, which is in agreement with experimental results obtained by Dequiedt [8,11].

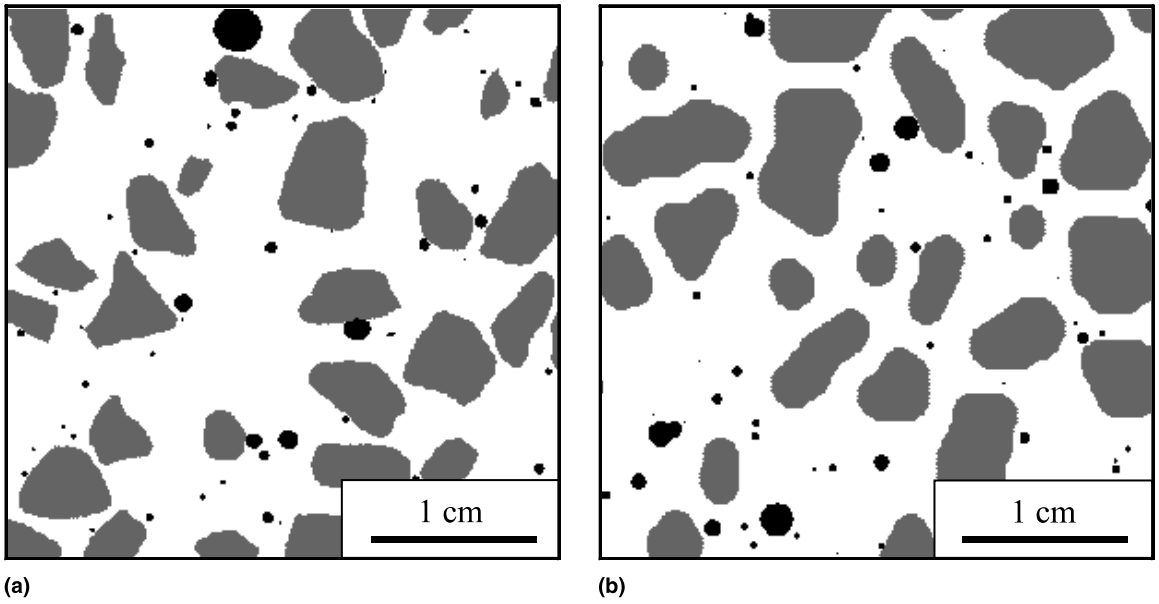

Fig. 10. Real and simulated image of the three phases in a concrete (series without AEA).

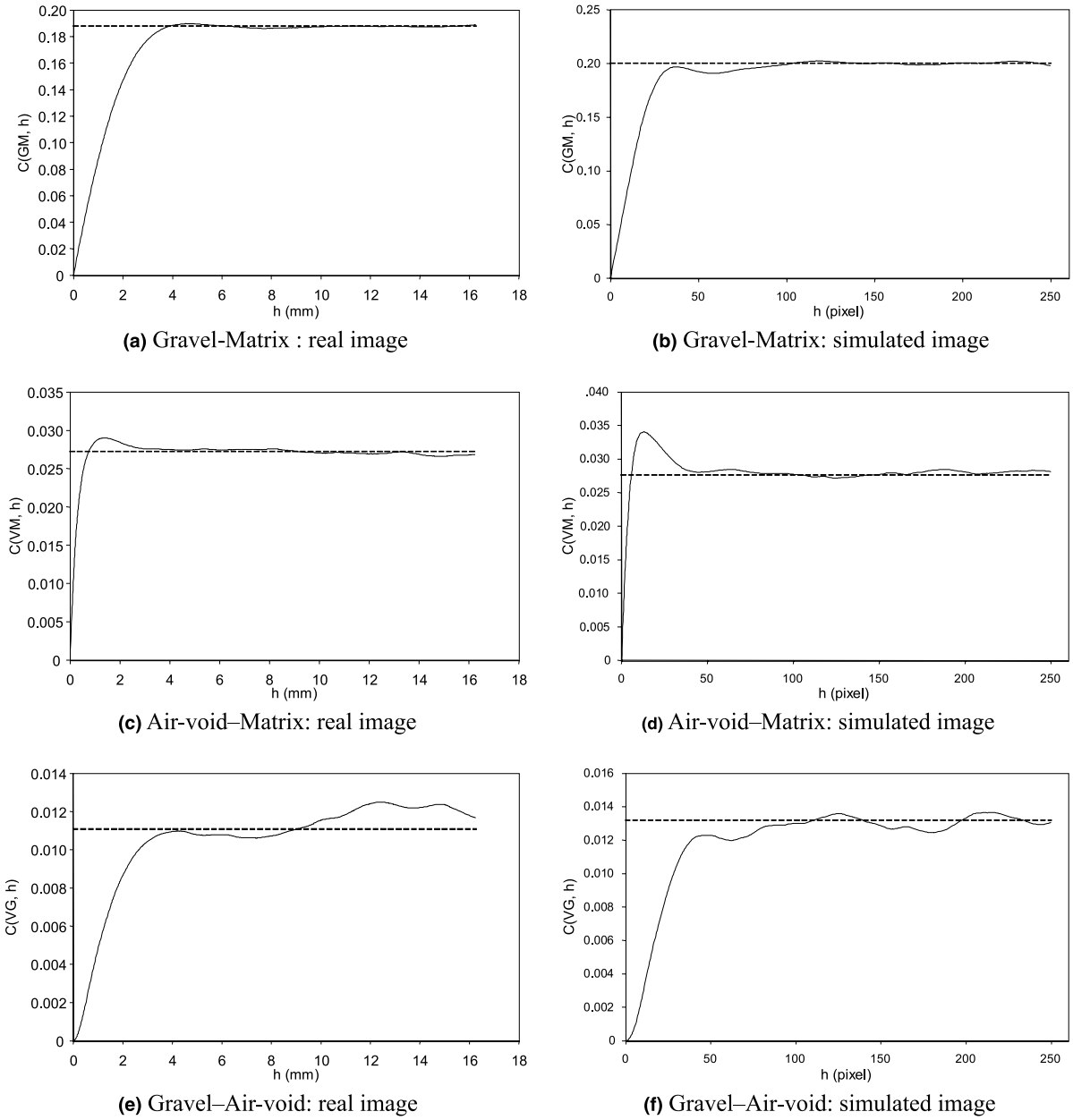

Fig. 11. Real and simulated crossed-covariances of the concrete series with AEA. $C(X_i : X_j, h)$ and $C(X_j : X_i, h)$ covariances are gathered. With G: gravel; M: matrix, V: air-voids.

Figures 11(b), (d) and (f) show the simulated crossed-covariances for the series with AEA. They can be visually compared with the plots obtained from real images Figs. 11(a), (c) and (e). Of course, the curves cannot be superimposed, but there are some similarities:

- the local maximum exists both for the covariance between air-voids and matrix, and between gravel and matrix,
- the covariance between gravel and air-voids is the most irregular,
- the specific surface area of contacts calculated from the slopes at the origin are relatively comparable between real and simulated images (Table 2): in particular the specific surface area of contact between air-voids and gravel is practically zero, which means that the specific surface areas of contact between on the one hand air-voids and matrix and on the other hand gravel and matrix are close to the total specific surface areas of air-voids and of gravel.

Of course, there exists other types of models which have been developed to simulate a microstructure: one can quote those based on computer-simulated grain structure [17–21], on mosaic patterns [22], on discrete numerical modelling and packing of spheres [23,24], even

Table 2
Specific surface area of contact between the analyzed phases from crossed-covariances

	Real images		Simulated images	
	Without AEA	With AEA	Without AEA	With AEA
$S_V(GM)$ (mm^{-1})	0.42	0.41	0.40	0.40
$S_V(VM)$ (mm^{-1})	0.15	0.31	0.13	0.27
$S_V(GV)$ (mm^{-1})	0.003	0.005	0.002	0.004

on a microstructural scale, using image processing defined on a finite element method (FEM), [25], or etc. Some of these models can describe microstructures of concrete materials, more or less correctly. Using probabilistic models, visual similarities of the microstructure and results on the crossed-covariances between the different concrete phases give an excellent agreement between real and simulated mesostructures in $\mathbb{R}^2$.

5. Conclusion

The scope of these experimental results on the modelling of a Boolean model of disks and of a Voronoi tessellation was intended to set the first milestones for a model on a complex material such as concrete. It appears that such a procedure is correct.

If the Boolean model has good stereological properties, it is not the same with the Voronoi tessellation used to model gravel. The research of a complete model in $\mathbb{R}^3$ will necessitate a 3D simulation and, therefore, to make random plane sections of this 3D structure [26].

From our work, one cannot conclude that the proposed model corresponds precisely to bulk material, but in 2D space, these is a very good agreement between results on real materials and simulation. It is the first step in this direction and the method must be refined, particularly to be extended for 3D space by a way which seems easy to imagine. This opens up a new, very promising, approach of research.

Acknowledgements

This work was performed in the frame of the "Pôle Traitement et Analyse d'Images", Pôle TAI, (Pole of Image Processing and Analysis) of Basse-Normandie, France. Concrete specimens were elaborated at ESITC, Groupe ESTP, Epron: we want to thank this School of engineers for allowing us to use their facilities.We want to thank the Ministère de l'Education Nationale, de la Recherche et de la Technologie (MENRT) for a fellowship (ASD).

References

[1] De Hoff RT, Rhines FN. Quantitative microscopy. New York: McGraw-Hill; 1968.
[2] Underwood EE. Quantitative stereology. Reading (MA): Addison Wesley; 1970.
[3] Coster M, Chermant JL. Précis d'analyse d'images. Paris: Les Editions du CNRS; 1985 (2nd ed., Paris: Les Presses du CNRS, 1989).
[4] Serra J. Image analysis and mathematical morphology. London: Academic Press; 1982.
[5] Jeulin D. Modèles morphologiques de structure aléatoires et de changement d'échelle. Thèse de Doctorat ès Sciences, University of Caen, 1991.
[6] Pigeon M, Plante P, Saucier F. Production et stabilité du réseau de bulles d'air entraîné dans le béton. Report of the University Laval, Département de Génie Civil, April 1987.
[7] Pleau R, Pigeon M, Laurencot JL. Some findings on the usefulness of image analysis for determining the characteristics of the air-voids system on hardened concrete. Cem Concr Comp 2001;23:237–46.
[8] Dequiedt AS. Contribution à l'étude morphologique des ciments et bétons par analyse d'images multimodales. Thèse de Doctorat of the University of Caen, 1999.
[9] Dequiedt AS, Redon C, Chermant JL, Chermant L, Coster M. Characterization of diffusion paths of water in concrete by color image analysis. Acta Stereol 1999;18:227–37.
[10] Dequiedt AS, Coster M, Chermant L, Chermant JL. Study of phase dispersion in concrete by image analysis. Cem Concr Comp 2001;23:215–26.
[11] Dequiedt AS, Coster M, Chermant L, Chermant JL. Distance between air-voids in concrete by automatic methods. Cem Concr Comp 2001;23:247–54.
[12] Choquet G. Theory of capacities. Ann Inst Fourier 1953;5:131–295.
[13] Matheron G. Random sets and integral geometry. New York: Wiley; 1975.
[14] Coster M, Chermant JL. Image analysis and mathematical morphology for civil engineering materials. Cem Concr Comp 2001;23:133–51.
[15] Matheron G. Eléments pour une théorie des milieux poreux. Paris: Masson; 1967.
[16] Jeulin D. Morphologie mathématique et propriétés physiques des agglomérés de minerai de fer et du coke métallurgique. Thèse de Docteur-Ingénieur, Ecole des Mines de Paris, 1979.
[17] Garboczi EJ, Bentz DP. Computational materials science of cement-based materials. Mater Res Bull Soc 1993;18:50–4.
[18] Bentz DP, Garboczi EJ, Martys NS. Application of digital-image based models to microstructure transport properties and degradation of cement-based materials. In: Jennings H, Kropp J, editors. The modelling of microstructure and its potential for studying transport properties and durability. Dordrecht: Kluwer Academic Publishers; 1996. p. 167–85.
[19] Bentz DP. Three-dimensional computer simulation of Portland cement hydration and microstructure development. J Am Ceram Soc 1997;80:3–21.
[20] Mehnert K, Ohser J, Klimanek P. Testing stereological methods for the estimation of spatial size distribution by means of computer-simulated grain structures. Mater Sci Eng 1998;A246:207–12.
[21] Nippe M, Ohser J. The stereological unfolding problem for systems of homothetic particles. Pattern Recognition 1999; 32:1649–55.
[22] Xi Y, Tennis PD, Jennings HM. Mathematical modeling of cement paste microstructure by mosaic pattern. Part I: Formulation. J Mater Res 1996;11:1943–52.

[23] Stroeven M. Discrete numerical modelling of composite materials: application to cementitions, materials. Ph.D. thesis, Technische Universität Delft, 1999.
[24] Dinger DR. One-dimensional packing of spheres – Part II. Am Ceram Soc Bull 2000;79:83–91.
[25] Gokhale AM, Yang S. Application of image processing for simulation of mechanical response of multi-length scale microstructures of engineering alloys. Met Mater Trans 2000;A30:2369–81.
[26] Decker L, Jeulin D. Simulation 3D de matériaux aléatoires polycristallins. Rev Met CIT Sci Génie Mater 2000;97:271–5.